Effect of thermo-oxidative ageing on the rheological properties of bituminous binders and mixes: Experimental study and multi-scale modeling

Saannibe Ciryle Somé, Jean-François Barthélémy, Virginie Mouillet, Ferhat Hammoum, Gang Liu

Version of Record: https://www.sciencedirect.com/science/article/pii/S0950061822019225
Manuscript_9df794b0bb2bdca1f3040c0d4c3e6cbd

Effect of ageing kinetics on the rheological properties of bituminous binders and mixes: experimental study and multi-scale modeling

C. Somé[1], J-F. Barthélémy[1], V. Mouillet[2], F. Hammoum[3], and G. Liu[4]

[1]Cerema, Univ Gustave Eiffel, UMR MCD, F-77171 Sourdun, France
[2]Cerema, Univ Gustave Eiffel, UMR MCD, F-13100 Aix-en-Provence, France
[3]Université Gustave Eiffel, Laboratoire MIT, Route de Bouaye - CS 5004 - 44344 Bouguenais
[4]State Key Laboratory of Silicate Materials for Architectures, School of Materials Science and Engineering, Wuhan University of Technology, Wuhan 430070, China

Abstract

The oxidative ageing of hot mix asphalt (HMA) and foamed warm mix asphalt (WMA), performed through laboratory accelerated ageing processes is investigated in this study. 50/70 pen-grade bitumen is used to produce the mixes. Four ageing durations (0, 3, 6 and 9 days) are considered to investigate the kinetics of long-term ageing based on a RILEM ageing procedure. The binders of the aged mixes are extracted and characterized. Moreover, RTFOT and PAV tests are carried out on fresh bitumen to simulate the long-term ageing of HMA and WMA. Rheological tests are performed at different temperatures and frequencies to determine the stiffness moduli of binders and mixes that are subsequently curve-fitted with the modified 2S2P1D model. The results show that the stiffness moduli of binders and mixes increase with the long-term ageing duration. This increase is more pronounced for WMA and their binders than HMA. Moreover, the increase of the stiffness modulus is shown to be related to parameters such as asphaltene content, carbonyl and sulfoxide indices. Finally, a multi-scale model which combines the Mori-Tanaka scheme at mastic and mortar scales and the self-consistent scheme at the mixture scale with possible grain-grain contact between the coarse aggregates, is implemented. It is able to account the evolution of the master curves of the stiffness moduli $|E^*|$ and the phase angles δ of the mixes based on bitumens' and aggregates' properties. The reliability of this multi-scale model is assessed through a comparison with experimental data, over a wide range of frequencies and temperatures.

keywords: bituminous mixture, ageing, stiffness modulus, multiscale modeling

1 Introduction

Bituminous mixes are viscoelastic complex composite materials build up from a mixture of aggregates, bitumen, fillers and additives. As such, their end performances entirely depend on

their component percentage and properties, their interaction with each other and the evolution of their properties other time. Many parameters have a significant influence, such as aggregate size and grading, filler size distribution, bitumen properties and the interaction between bitumen and aggregates. Understanding the influence of all these parameters is a challenging task and requires a multi-scale modeling to assess the effect of each component [1, 2, 3]. Moreover, the ageing induced by the manufacturing and the field climatic conditions modifies the chemical composition of the binder that makes the mixes' performances to evolve. Indeed, the ageing of mixes occurs in two main stages: the short-term ageing is caused by the manufacturing in the mix plant, the transport and the paving where the ageing process is mainly linked to the departure of the volatile compounds of bitumen, while the long-term ageing which occurs during the pavement service life is influenced by climatic conditions and road traffic. The latter is related to the steric hardening, oxidation and UV rays that affect only the 12 mm upper layer of the roads [4].
In order to simulate the ageing that takes place over several years, many accelerated ageing methods are developed in laboratory. Among those methods, one can distinguish on the one hand, the ageing processes on bitumen such as the Rolling Thin Film Oven (RTFO)[5] followed by the Pressure Ageing Vessel (PAV) [6] which is claimed to reproduce 7 to 10 years natural ageing of an bituminous pavement [7]) and on the other hand those carried out on loose or compacted mixes. The Table 1 summarizes the common ageing protocols of loose mixes. But to our knowledge there is no equivalence between these latter and the RTFOT+PAV ageing methods that can be performed on bitumens while both ambition to predict the in situ ageing. The prediction of field ageing based on laboratory protocols is still questionable and imprecise. Most of the accelerated ageing methods developed in laboratory simulate between 5 and 10 years ageing on the in-situ pavements [4, 8, 9, 10]. In general, the predictions are more or less based on the analysis of one of the following indicators: carbonyl or sulfoxide indexes [4], rheological properties, mechanical performance but never all indicators together.
The protocols to simulate the long-term ageing of warm mixes are still under investigations. Only Raab et al. [11] developed a laboratory ageing protocol for warm mixes using compacted specimen.

In this context, the present work deals with the ageing kinetics of HMA and WMA investigated through the RILEM ageing protocol. The paper focuses on the impact of several long term ageing duration on the rheological and chemical properties of bitumens extracted from mixes aged in accordance to the RILEM ageing protocol on loose mixes [10], i.e. loose mixture aged during 4 hours of at 135C follow by 9 days ageing of the mixture at 85C (as reported in the european Technical Specification CEN TS 12697-52 [19]). Moreover, pure bitumens is aged according to the RTFOT (EN 12607-1 [5]) and PAV (EN 14769 [6]) methods to compare the results with the RILEM ageing method [10].
A part of this study also focuses on multi-scale modeling of the rheological properties of the aforementioned mixes (HMA and WMA) based on the morphology of their microstructure and the properties of theirs constituents (bitumens, aggregates, air voids). In the last decade, micromechanical tools [25, 1, 2, 26, 27, 28, 1, 29, 3] and discrete element methods (DEM) [25, 30, 31, 32] gains more interest in the bituminous mix community. In the DEM approach, the contact between aggregates is modeled by the viscoelastic Burger's model which accounts for the linear viscoelastic $l.v.e$ behavior of the bitumen that coats the aggregates, while in the micromechanical approach the generalized self-consistent scheme (GSCC) is claimed to be an efficient model to model the $l.v.e$ of bituminous mixes [1, 2, 3]. Other micromechanical models

Loose mixture					
	Short-term Ageing		Long-term Ageing		Field
Ageing Procedure	Temp. (^{o}C)	Duration	Temp. (^{o}C)	prediction	
Van Gooswilligen 1989 [12]	-	-	160	16h	
Shell (Read and Whiteoak 2003) [13]	Mixing Temp.	2h	80	7 days	
LCPC (Such 1997) [14]	135	4h	100	24 h	
RILEM TG5 2009 [10]	135	4h	85	9 days	-
BRRC [15]	135	1.5h	60	14 days	
Re-Road project [16]	135	4h	90	20h	
Van den Bergh (2012) [17, 18]	135, 130	4h, 3h	85, 90	7 days	
TS 12697-52 [19]	135	4h	85	9 days	
India 2019 [4]	135	4h	85	9 days	122h $\Rightarrow$ 5 years
Compacted specimen					
	Temp. (^{o}C)		Duration		Field
TRL (Nicholls 2006) [20]	110-120		48 h		
EMPA (Van den Bergh 2011) [18]	60		16 h		
SHRP-A-390 [21] [8]	85		5 days		5-10 years [8]
Nottingham Univ. [22]	85		65 h		-
Japan 2003 [23]	70		0-8 days		-
Tia et al. (1988) [24]	60		90 days		
Raab 2017 [11]	66h at 85 ^{o}C + 6h at 20 ^{o}C+42h at 85^{o}C +6h at 20^{o}C +42h at 85^{o}C +6h at 20^{o}C +66h at 85^{o}C				
Loose mixture and compacted specimen					
	Short-term Ageing (Loose mixture)		Long-term Ageing (compacted mix)		Field
The Netherlands [9]	165 ^{o}C	2h	90^{o}C	7 days	10 years
	135^{o}C	4h	135^{o}C	40h	10 years

Table 1: Loose mixes ageing protocols

have been developed by Zhu et al. [26] and Shu et al.[27]. The model developed by Zhu et al.[26] predicts the elastic modulus of asphalt mixes taking into account the imperfect bonding between the aggregate and the bituminous mastic layer. The imperfect bonding at the interface is modeled by a spring. The spring stiffness varies from 10 to 10^8 and is used as a setting parameter that allows the model to fit the experiments. It is shown that a value of k=50 allows a good fitting of the experiments. Shu et al. [27] developed a 2-layers micromechanic model in 3D taking into account the aggregates gradation and a film of bituminous mastic that coats the aggregates, to predict the dynamic modulus of polymeric bituminous mix. They assumes that every aggregate is coated with the same thickness of bituminous mastic contrary to the works of Duriez [33]. Their model fails to predict the dynamic modulus of asphalt concretes mixtures. The reasons for the discrepancy between measured and predicted dynamic moduli are discussed in their paper.

In all the previous works the comparison between the model and the experiments are often limited to a narrow range of temperature and frequency [28, 1, 2, 27, 26]. In particular, previous models cited fail to predict viscoelastic properties at temperatures above 20^{o}C.

The micromechanical approach adopted in this study is inspired by the micro, meso and macro scales presented in [1]. The micro-scale is characterized by the bituminous mastic whereas the bituminous mortar is considered at the meso-scale level. At these levels a Mori-Tanaka scheme is used, while the macroscopic scale (bituminous concrete level) is modeled by a generalized self-consistent scheme (GSCC) based on the solution of the composite sphere in an infinite matrix provided in [34]. However, the use of Mori-Tanaka scheme at the meso-scale is questionable since the inclusion fractions represented by the fine aggregates is very higher than the mastic fraction that play the role of matrix. In addition the new model presented in this paper aims at improving previous ones by taking into account the stiffening effect of grain contacts which play a crucial role at high temperature or low frequency.

This article is organized in two main parts:

- Section 2 presents on the one hand the mix design and the evaluation of the bituminous mastic layer that coats coarse aggregates, and on the other hand, it describes the ageing protocols of hot and warm mixes and the bitumens;
- Section 3 describes the rheological tests performed to evaluate the linear viscoelastic ($l.v.e.$) properties of the binders and mixes;
- Section 4 presents the results of the chemical analysis of the carbonyl and sulfoxide indices that characterize the ageing of the binders;
- Section 5 presents the multiscale modeling of the complex modulus of the mixes based on aggregate and bitumen properties and the comparison between models and experiments.

2 Materials and mix design

2.1 Materials properties

The mixes are produced with a paving grade bitumen 50/70, whose properties of needle penetration (EN 1426) and softening temperature (EN 1427) are respectively 57 $\times$ 0.1 mm and 49.6 ^{o}C, and porphyry aggregates which come from *Pont de Colonne* quarry (in France) whose abrasion loss and fragmentation properties respectively known as Microdeval (EN 1097-1) value and Los Angeles (EN 1097-2) value are 17% and 8%. The aggregate gradation used in the AC10 mixture (according to the EN 13108-1 [35]) is presented in Fig. 1. It is used for surface and binder courses. The mixture composition and the densities of the constituents are given in Table 2. The mixture is produced using a laboratory mixer considering the optimum binder content of 5.4%, previously determined.

Constituent	Mass content (in %)	Density (in $kg.m^{-3}$)
Limestone filler	2.96	2700
0/2	27.59	
2/6.3	25.05	2700
6.3/10	44.4	
Bitumen 50/70	5.4	1040
Cecabase for WMA	1% (bitumen mass)	900

Table 2: Mix composition

2.2 Evaluation of bitumen layer around the aggregates

The interest of this preliminary section is to evaluate the thickness of the mastic film that coats the aggregates, given that this parameter is important for the future multiscale modelling. To do this, we use the successive bitumen recovery method on bituminous mixture fractions already sieved. This procedure was previously used by Marius Duriez [33] to determine the thickness of the bitumen film around aggregates.

Thus, to evaluate this bituminous mastic thickness, bituminous mixture 0/10 is manufactured, loosen and spread in thin layer. After cooling, they are sieved to obtain 5 batches of

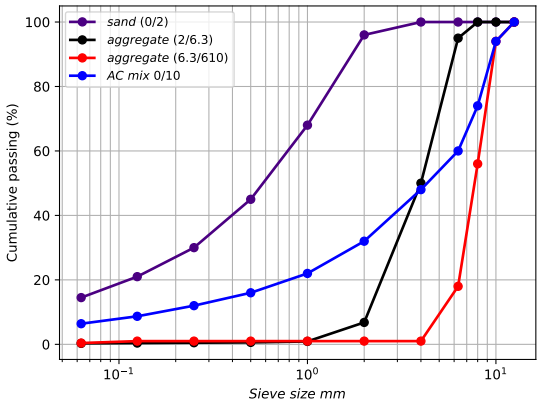

Figure 1: Grading curve of the AC mixture aggregate

bituminous mixtures fractions: 0/2, 2/4, 4/6.3 6.3/10, 10/14 as shown in Fig. 2(a). The bitumen amount of each fraction is recovered as described in section 2.4.3. It should be noted that small fractions of bituminous mixes can agglomerate or stick to coarser aggregates. Thus, each fraction contains the fractions of smaller diameters; for example the fraction of bituminous mixes 4/6 contains aggregates 4/6, 2/4, and 0/2. After the bitumen recovery the batch of aggregates of each bituminous mixture fractions is sieved again. For the fraction 0/2 of the mixture, it is easy to determine the bitumen content after the bitumen recovery. For the other mixes fractions, we proceed recursively by first determining the amount of bitumen in the fraction 0/2 then in the 2/4 contained in the mixture 2/4. Then, we proceed similarly for mixture 4/6.3, 6.3/10 and 10/14 successively. The bitumen content evaluated in each aggregates fractions are given in Table 3.

Constituent	Mass content (in %)
0/2	10.31
2/4	4.29
4/6.3	3.62
6.3/10	2.36

Table 3: Bitumen content in each granular fraction

Once the bitumen content of each aggregate fraction is known, we assume the aggregates as spherical then we determine the bitumen layer thickness around each aggregate as follows:

$$e_{mastic}^{nominal}(d_i) = \frac{B_C}{S \times \rho_b} \tag{1}$$

where B_C is the bitumen content of each aggregate fraction, ρ_b is the bitumen density and S the specific surface of the aggregate defined as the ratio of the surface over the mass of the aggregate: $S = 6/(d \times \rho_g)$ where ρ_g is the aggregate density and d_i accounts for the mean diameter of each fraction i.
By applying this approach, we obtain the following relationship:

$$e_{mastic}^{nominal}(d_i) = e_0 \times (d_i/d_0)^{0.513} \text{ where } d_0 = 1 \text{ mm and } e_0 = 61.3 \text{ µm} \tag{2}$$

Eq.2 assumes that all the bituminous mastic recovered from experiment is used to coat the sands and coarse aggregates. This is not totally true because only a part of this mastic is used to coat the coarse aggregates and the other part is used to form the bituminous mortar (with the sands) that fills partially the intergranular pores. An estimation of the distribution of this bituminous mastic between the inter-granular mortar and the coated aggregates is presented in section 5.2.1.

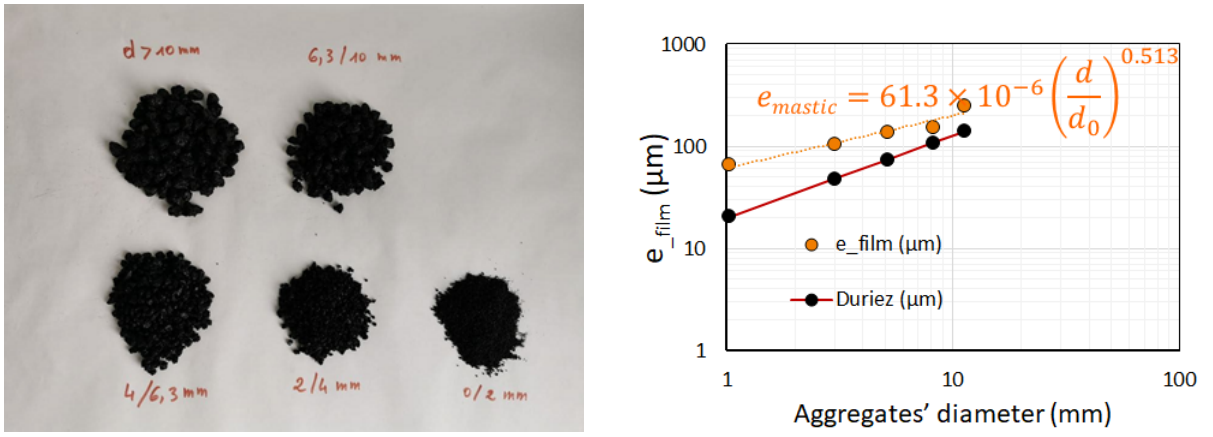

(a) AC10 mixture fractions

(b) evolution of e_{film} according to the diameter

Figure 2: Evaluation of bitumen layer around the aggregates

2.3 Ageing of bituminous mixture

The RILEM ageing procedure on loose mixture is adopted in this section instead of ageing of compacted specimens. This choice is motivated by the following reasons:

- air and heat can easily circulate inside the bituminous mixture, thus, allowing uniform ageing throughout the mixture
- the risks associated with the loss of integrity of the compacted samples (risk of creep) during laboratory ageing can be reduced
- the rate of oxidation may increase due to exposure to oxygen from a larger binder surface.

2.3.1 Ageing of hot mix asphalt (HMA)

The hot mixes AC 0/10 is manufactured at 165^{o}C and then subjected to different ageing duration from 0 to 9 days. After the mixing, the loose HMA mixture is cooled down to 135^{o}C and spread in thin layer into a tray (not more than 2.5 cm to favor better circulation of air around the coated aggregates to accelerate the ageing process) and placed in a ventilated oven during 4 hours to simulate the short term ageing. Then, it is cool down to 85^{o}C and kept in the oven for 3, 6 or 9 days to reproduce the long term ageing. At the end of the ageing procedure the loose mixes is reheated at 135^{o}C during 2 hours then compacted. The reference hot mix is compacted just after the mixing without long-term ageing and designated H0 while those subjected to long-term ageing is labeled H3, H6, H9 corresponding to the 3, 6 or 9 days ageing.

The various stages as well as the temperatures involved are shown schematically in Fig. 4.

In addition, in order to later validate the multi-scale model at the mortar scale, a mortar bituminous mixture AC 0/2 is manufactured at 165^{o}C and compacted without short and long term ageing using the bitumen content of 10.31% as determined in Table 3. It is designated M_0. For this operation the limestone fillers added to the 0/2 aggregates fractions are presented in Table 2.

2.3.2 Ageing of foamed warm mix asphalt (WMA)

The foamed bitumen is produced by mixing bitumen preheated to 165^{o}C, 1% of Cecabase additive and 5.5% of added water initially kept at ambient temperature. Preliminary investigations show that this procedure allows to obtain maximum expansion ratio of the foam equal to 45 times the initial bitumen volume. The foam is produced at the outlet of the tank by adjusting the flow rate of water and bitumen and instantly sprayed under pressure onto the aggregates which are preheated to 135^{o}C. These components are mixed to obtain a better coating of the aggregates. The foam and mixture produced with the Wirtgen WBL 10S apparatus which allows automatic control of temperatures, water and bitumen flow rate and foam injection pressure. The WMA is manufactured at 135^{o}C then immediately spread in thin layer. The short and long term ageing and compaction procedures applied are similar to that of HMA (see also Fig. 4). The mixes manufactured is labeled W0, W3, W6, W9 for reference (0), 3, 6 or 9 days ageing respectively.

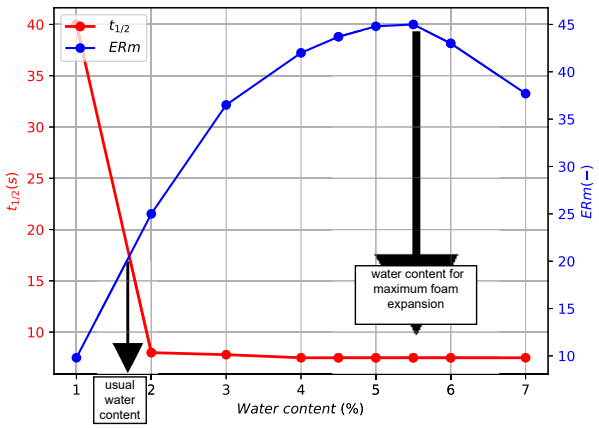

Figure 3: Determination of the optimal water content for bitumen foaming

2.4 Ageing of bitumen

2.4.1 Simulation of HMA field ageing by RTFOT and PAV protocols

The RTFOT [5] and PAV [6] ageing protocols are carried out on fresh bitumen to simulate respectively the short-term and long-term ageing that a binder undergoes during HMA production until paving and its natural ageing during the service life. The RTFOT is carried out at 163^{o}C during 75 min according to EN 12607-1. The long-term ageing of HMA is simulated

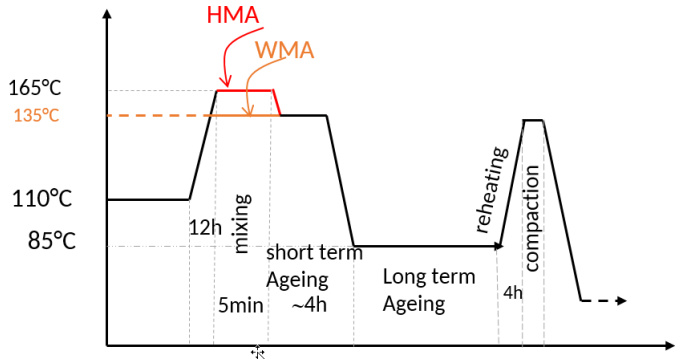

Figure 4: Ageing kinetic of HMA and WMA used in the current study

using the pressure ageing vessel (PAV) test in accordance to the EN 14769. It is supposed simulate 7 to 10 years ageing on the road during the life time of the pavement [7].

2.4.2 Simulation of WMA field ageing by RTFOT and PAV protocols

The short term ageing of WMA is simulated by the RTFOT performed at a temperature of 140^{o}C other parameters remaining unchanged. This temperature is selected in order to be the closest to the manufacturing temperature of WMA. The long-term ageing of HMA is simulated using PAV procedure in accordance to the EN 14769.

2.4.3 Bitumen recovery

First of all, an important step before binder's characterization is the binder's extraction and recovery of bituminous samples, carried out according to the following experimental procedure described in the French testing method [36]: the pavement cores of bituminous mixtures are broken into small pieces before solvent extracting the binder from the aggregates. The extraction is based on the dissolution in the dichloromethane solvent at room temperature. This binder solution is then filtered and centrifuged to remove all aggregate particles from the binder solution. After that, the solvent is removed by distillation under air vacuum. It is important to note that after the binder is extracted and recovered, it is analysed by infrared spectroscopy to ensure complete solvent removal (no infrared peaks of chlorine) and the calcination residue during 8 hours at 450^{o}C has to be less than 1% of binder test portion. After complete solvent removal, a physico-chemical and rheological studies could be performed on recovered binders aged at different levels

The RTFOT and RTFOT+PAV aged bitumens and those recovered from the mixes (H0 to H9, W0 to W9) is tested with dynamic shear rheometer (DSR).

3 Rheological tests

3.1 2-point cantilever beam test

The complex modulus E^* of the mixes is carried out on a prismatic cantilever bending test in accordance to EN 12697-26 (Annex A: 2P-PR [37]) varying the temperature from -10^{o}C to 50^{o}C and the frequency from 3 Hz to 40 Hz. The test is carried out by applying a sinusoidal

deflection $z = z_0 \sin(\omega \times t)$ to the head of a specimen glued at its base to a stand fixed to a rigid chassis. The deflection z_0 is such that it causes a strain $\epsilon \leq 50 \times 10^{-6}$ in the most heavily stressed part of the specimen, which is supposed to correspond with the linear range of the bituminous mixture. The force F and the phase angle δ measured allow to calculate the real and imaginary component (respectively E_1 and E_2) of the complex modulus as follows:

$$E_1(\omega) = \gamma \left(\frac{F_0}{z_0} \cos(\delta(\omega)) + \mu \times \omega^2 \right); E_2(\omega) = \gamma \frac{F_0}{z_0} \cos(\delta(\omega)) \tag{3}$$

Where $\gamma = 4L^3/(bh^3)$ is the form factor which depends on the specimen form and $\mu = M/4 + m$ is the mass factor which is a function of the mass of the specimen, M, and the mass of the movable part, m that influence the resultant force by their inertial effects. Then, $|E^*| = \sqrt{E_1^2 + E_2^2}$ and $\delta = \arctan(E_2/E_1)$. The isotherms of $|E^*|$ and δ are then used to built the master curves (see section 3.3).

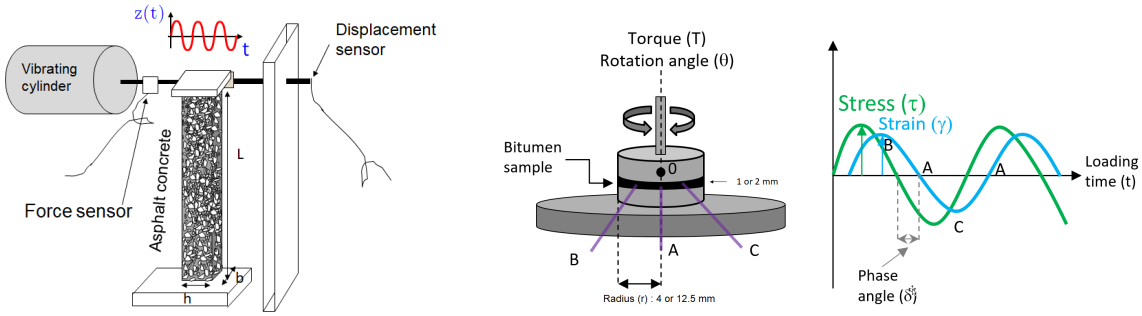

(a) Mixes complex modulus $E^*(\omega)$ test principle

(b) Bitumen complex modulus $G^*(\omega)$ test principle

Figure 5: Evaluation of rheological properties

3.2 Dynamic Shear Rheometer test

The dynamic shear rheometer (DSR) is used to characterize the viscous and elastic behavior of bituminous binders at medium to high temperatures. It is performed on virgin and recovered binders, following EN 14770 [38]. This test measures the complex shear modulus $|G^*|$ of a material through oscillatory type solicitation as displayed in Fig. 5(b). The complex shear modulus G^* contains several information including the storage modulus, G_1, and the loss modulus, G_2, related to each other through the phase angle δ. These values are frequency and temperature dependent.

$$G_1(\omega) = \frac{2M_t H}{\pi R^4 \theta} \cos\delta; G_2(\omega) = \frac{2M_t H}{\pi R^4 \theta} \sin\delta \tag{4}$$

Where R is the radius of the specimen, H the specimen thickness, θ is the rotation angle of the upper piston, M_t is the torque moment. Then, $|G^*| = \sqrt{G_1^2 + G_2^2}$ and $\delta = \arctan(G_2/G_1)$. The isotherms of $|G^*|$ and δ are then used to built the master curves (see section 3.3).
Before starting the DSR measurement, strain sweeps is performed to determine the linear viscoelastic region of the binder. The parameter of the DSR test are given in Table 4. The DSR test is performed over a temperature range from 10°C to 80°C and frequency sweep from 0.681 to

21.54 Hz. The norm of the shear modulus $|G^*|$ and phase angle δ measured are used to build the master curves represented in Figs.8.

Device	Diameter of the parallel plate (mm)	Gap (mm)	Temp. (^{o}C)	Frequency (Hz)
DSR	25	1	50 to 80	0.681 to 21.54
DSR	8	1.8	10 to 40	0.681 to 21.54

Table 4: Parameters of DSR test

3.3 Master curve building

The isotherms are shifted according to the procedure described in refs. [39, 40] to obtain the modulus ($|E^*(\omega)|$) and phase-angle $\delta(\omega)$ master curves at the reference temperature $T_{ref} = 10$ ^{o}C. This method of constructing the master curves is chosen because it is relatively simple to implement and above all, it allows to construct the master curves without introducing the errors that a manual translation of the isotherms can introduce. According to this method, which is based on Kramers-Kronig relationships between $|E^*(\omega)|$ and $\delta(\omega)$ [41], the shifting factors are calculated by the following expression:

$$\log(a_{(T_i,T_{ref})}) = \frac{\pi}{2}\sum_{j=i}^{j=ref}\frac{\log(|E^*(T_j,\omega)|) - \log(|E^*(T_{j+1},\omega)|}{\delta_{avr}^{(T_j,T_{j+1})}(\omega)}; i = 1, 2, ..., N \tag{5}$$

where $|E^*(T_j,\omega)|$ and $|E^*(T_{j+1},\omega)|$ are the norms of the complex moduli measured at consecutive temperatures T_j and T_{j+1} at the lowest frequency ω and $\delta_{avr}^{T_j,T_{j+1}}(\omega)$ is the average of the phase angles measured at T_j and T_{j+1} for the lowest frequency ω.

In practice, translation coefficients are calculated by taking the lowest experimental value obtained for ω and for each isotherm. Translation coefficients $a_{(T_i,T_{ref})}$ calculated using Eq.5 enable us to adjust coefficients C_1^{ref} and C_2^{ref} of the Williams Landel and Ferry law:

$$\log(a_{(T_i,T_{ref})}) = \frac{-C_1^{ref}(T_i - T_{ref})}{C_2^{ref} + T_i - T_{ref}} \tag{6}$$

Using this adjustment method, it is possible to obtain pairs of coefficients C_1^{ref} and C_2^{ref} for different reference temperatures $T_{ref'}$. If one compares these values with those deduced from passage laws as follows:

$$C_2^{ref'} = C_2^{ref} + T_{ref'} - T_{ref}; C_1^{ref'} = \frac{C_2^{ref} \times C_2^{ref}}{C_2^{ref'}} \tag{7}$$

A Python routine is implemented to build the master curves at a reference temperature of 10^{o}C. This routine is also used to calibrate the rheological model described in section 3.4.

3.4 Calibration of the rheological model

We use here the Huet-Sayegh model (2S2P) and the C. Such model (1S2P1D) that are some particular case of the 2S2P1D model formerly developed by Huet [42] to interpret the complex

modulus tests performed on bituminous materials then successively improved par several authors [43, 44, 14, 45]. It is represented by a purely elastic spring connected in parallel to two parabolic dampers (sensitive to temperature) in series with an elastic spring, as sketched in Fig. 6. In the frequency domain, the complex modulus of the modified Huet model reads [45]:

$$E^*(i\omega\tau) = E_0 + \frac{E_\infty - E_0}{1 + \delta(i\omega\tau)^{-k} + (i\omega\tau)^{-h} + (i\omega\tau\beta)^{-1}} \tag{8}$$

Where E_∞ denotes the glassy modulus when $\omega \to \infty$ and E_0 the static modulus when $\omega \to 0$; η; $\omega = 2\pi f$, f : the load frequency. $\eta = (E_\infty - E_0)\beta\tau$ corresponds to the Newtonian viscosity of the dashpot. k and h are exponents of the parabolic dampers ($1 \succ$ h $\succ$ k $\succ 0$), and δ is a positive non-dimensional coefficient which accounts the proportionality between the characteristic times of the two parabolic dampers. τ is a response time parameter which accounts for the equivalence principle between frequency and the temperature. The bitumen bulk modulus k^{bit}=2500 MPa is assumed as that of synthetic polymers according to the work of Tschoegl [41](page 521), while the tensile modulus E^* is calculated from the shear modulus G^* as follows:

$$E^* = \frac{9KG^*}{3K + G^*} \tag{9}$$

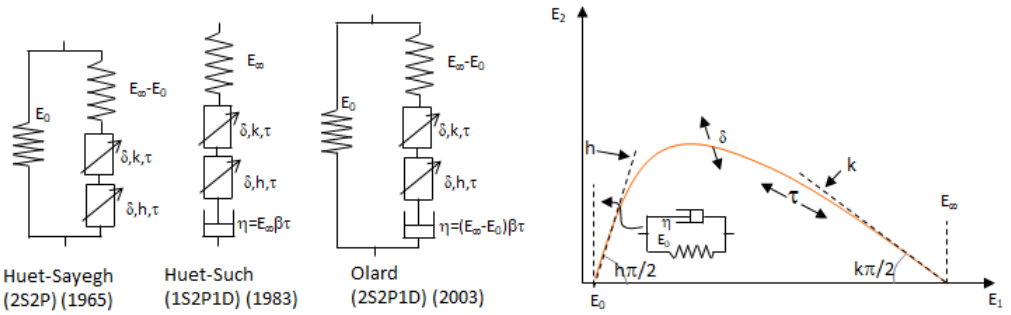

Figure 6: Thermo-viscoelastic 2S2P1D model

The optimization algorithm Subplex implemented in python nlopt library is used to calibrate the parameters of the rheological models. This calibration is done on the results of phase angle δ vs reduced frequency ($a_T\omega$) domain. The parameters obtained from this optimization are given in Table 5.
These parameters are obviously not universal, they depend on:

- The calibration of the parameters in other domain (cole-cole plan, Black space, or E^* vs reduced frequency ($a_T\omega$));
- The use of other optimization algorithms (Neldermead, Praxis, ...) ;
- The choice to fix or not the value of certain parameters during the optimization. E_∞ is kept constant in the data given in Table 5.

Let's precise that although they are not universal, the evolution of these parameters (in particular the increase of δ and τ) with ageing is in no way called into question.

The parameters E_0 and β in Eq.8 are related to the high temperature behavior, they are less precise since the experimental measurements are generally very scattered at high temperatures. The parameters E_0 and E_∞ are not considered, since they are almost partly exclusively dependent on the granular skeleton of a mixture rather than on the binder [45]. In addition, β is more relevant to high temperature behavior of the mixture. The parameter δ is shape parameter. It is called shape parameter in the Cole-Cole representation. τ is a characteristic time of the rheological model.

Mixes	E_0 (MPa)	E_∞ (MPa)	δ	τ (s)	k	h	
H_0	45	25000	1.85	0.52	0.21	0.61	
H_3	52	25000	2.68	1.88	0.19	0.61	
H_6	100	25000	3.17	4.78	0.19	0.59	
H_9	10	25000	3.42	7.63	0.19	0.59	
W_0	25	25000	1.98	0.38	0.19	0.61	
W_3	47	25000	3.77	7.37	0.19	0.61	
W_6	88	25000	3.68	101	0.19	0.59	
W_9	100	25000	3.0	1000	0.19	0.59	
Mortar M_0	49	25000	2.55	0.09	0.19	0.61	
Bitumen		E_∞	δ	τ	k	h	β
B_0		1800	2.89	3.65e-04	0.15	0.62	96
$B(RTFOT163)$		1800	2.81	9.55e-04	0.21	0.62	178
$B(RTFOT163+PAV)$		1800	4.90	4.83e-03	0.29	0.62	310
$B(H_0)$		1800	3.32	1.08e-03	0.21	0.62	145
$B(H_3)$		1800	3.60	1.32e-03	0.24	0.62	178
$B(H_9)$		1800	4.60	2.27e-03	0.24	0.62	221
$B(RTFOT140)$		1800	3.03	4.01e-04	0.19	0.62	145
$B(RTFOT140+PAV)$		1800	5.50	3.04e-03	0.26	0.62	278
$B(W_0)$		1800	5.56	5.16e-03	0.24	0.62	105
$B(W_3)$		1800	8.13	1.62e-02	0.26	0.61	288
$B(W_6)$		1800	9.78	3.93e-02	0.26	0.60	490

Table 5: Modified 2S2P1D model parameters for binders and mixes at $T_{ref} = 10\ ^o$C

3.5 Analysis of experimental results

Figs. 7(a), 7(c) show that the stiffness moduli of the mixes increase with the long term ageing duration. These increases in moduli result in a decrease of the phase angles as displayed in Figs. 7(b) and 7(d). The same observations can be made concerning the evolution of the moduli and phase angles of the bitumens extracted from the mixes (see Figs. 8(c) to 8(d)). The modified 2S2P1D parameters given in Table 5 show that the shape parameter δ and particularly the chacteristic time τ increase with the ageing duration when k, h and E_∞ are kept approximately constant. Thus, we can assume that the ageing mainly affects the characteristic time τ of binders and mixes. For the warm mixes and their bitumens, one can note that the characteristic times τ increase highly with ageing duration than HMAs and their binders. The results in the Table 5 show that the properties of warm mix W3 aged for 3 days are comparable to those of hot mix H9 aged for 9 days.

The higher ageing of WMAs is probably due to the higher water content of 5.5% used for the bitumen foaming. Usually this water content is less than 2% as shown in Fig 3 reducing the ageing WMAs [46]. Indeed, as shown in Fig 3, a high water content of 5.5% produces a higher foam volume that promotes good coating of the aggregates. However, a higher volume of foam bitumen implies a higher surface of bubbles of the foam exposed to air and subject higher oxidation since these have very thin thickness. In the case where the water content is relatively low, 1.8%, as in the work of Abbas et al.[46], the foam volume is lower, which leads to less oxidation. Viscosity measurements made by Li et al.[47] on soft bitumens (needle penetration of 75 × 0.1mm) after foaming with 1 to 5% water content, have shown that the viscosity increases for higher and lower water content while it decreases for medium water contents (3%). Even if they did not investige the ageing of the foam bitumen in their study, they show that a high water content can lead to counter-intuitive results on the properties of bitumens after foaming. Fig.8(c) also shows that RTFO test simulates quite well the short term ageing of HMA (H0) as already shown by literature [14]. However, the long term ageing simulated by the RTFOT at 163 ^{o}C + PAV is more severe than the RILEM long term ageing procedure at 9 days on loose mixes. Regarding the WMA, the RILEM ageing procedure on loose mixes is more severe than the RTFOT at 140^{o}C and RTFOT at 140^{o}C+PAV. The $|E^*|$ of the bitumen extracted from short term aged mixture W0 is similar to that of the RTFO at 140^{o}C+PAV which is supposed to simulate the long term ageing. In addition, it should be noted that the complex modulus of the bitumen recovered from W9 is not tested because the latter is too hard.

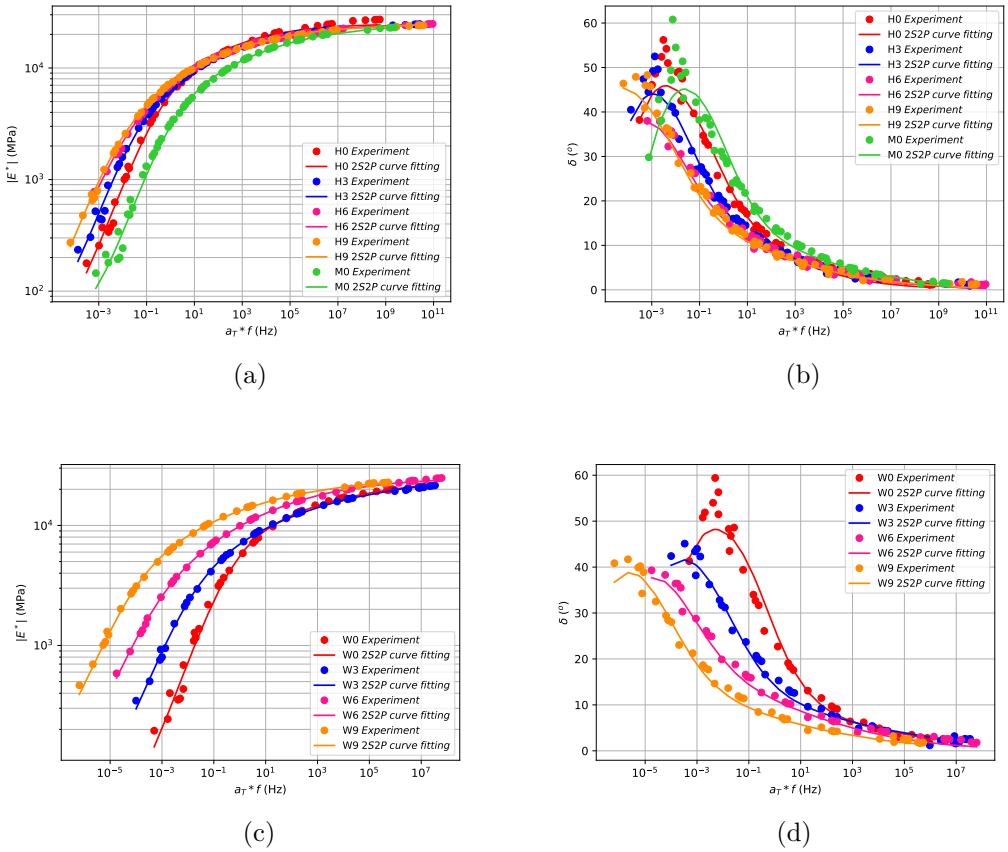

Figure 7: Master curves of complex moduli and phase angle of mixes at $T_{ref} = 10$ ^{o}C

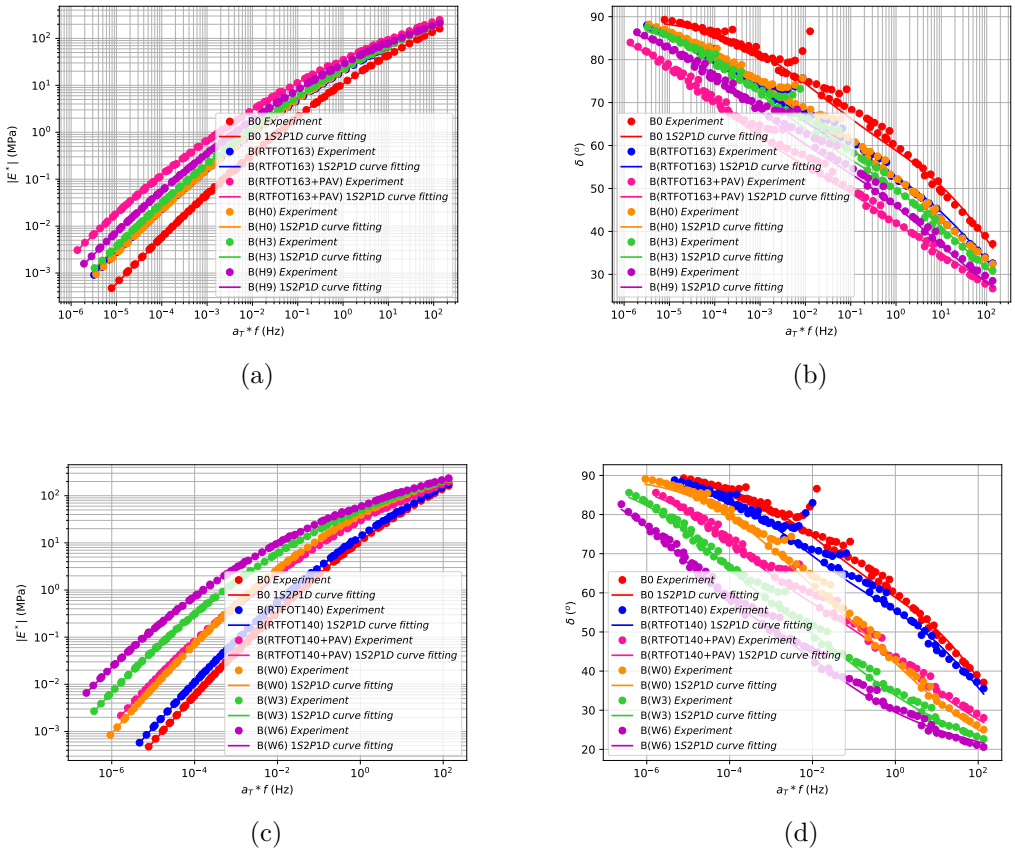

Figure 8: Master curves of complex moduli and phase angle of binders at $T_{ref} = 10^{o}$C

Fig.9 shows the evolution of the characteristic time τ with the ageing duration for binders and mixes. These results show higher slopes of τ in the case of WMAs compared to HMAs. The same observation applies to the recovered binders. This is consistent with the accelerated ageing WMAs due to bitumen foaming as explained previously. It is also noted that the characteristic times of asphalt mixes are 10 times greater than those of bitumens. This is mainly due to the presence of aggregates in the mixes and incidentally to the rheological model used to model the complex moduli of bitumens (1S2P1D) and that used for mixes (2S2P) and also to the optimization procedure (the boundary conditions on the modified 2S2P1D parameters during the optimization can differ from HMA to WMA on the one hand and also for binders recovered from HMA and WMA on the other hand).

4 Physico-chemical properties of aged bitumens

From a chemical point of view, ageing is caused by irreversible oxidation, itself due to the presence of oxygen in air, thus creating carbonyl ($C = O$) and sulfoxide ($S = O$) groups, modifying bitumen composition (increase in molecule size, bitumen polarity and aromaticity) and hardening the bituminous binder which becomes more brittle. Carbonyl and sulfoxide groups are considered as relevant markers for qualifying bitumen ageing and their monitoring by FTIR spectroscopy is often used. Sulfoxide groups can be present before ageing, according to the

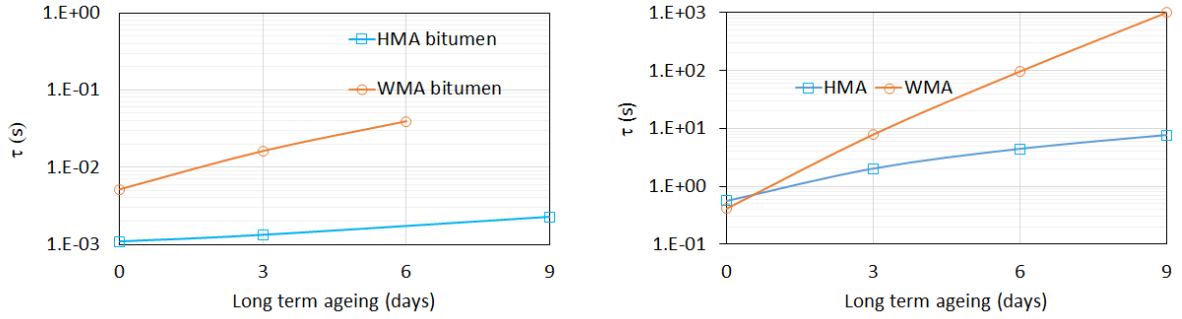

(a) (b)

Figure 9: Effect of long term ageing on characteristic time τ of the rheological 2S2P1D model

origin of crude oil. They form faster and at higher temperature than carbonyl groups. The determination of carbonyl or sulfoxide indexes (noted $I_{C=O}$ and $I_{S=O}$ respectively throughout this paper) by FTIR spectroscopy is used as a scientific tool in many research works to follow during time the ageing evolution of unique bitumen. In a FTIR spectrum, carbonyl and sulfoxide peaks are located at wavenumbers of 1700 and 1030 cm^{-1} respectively. $I_{C=O}$ (respectively $I_{S=O}$) is calculated as the ratio of the peak area of carbonyl (respectively sulfoxide) group centred at 1700 cm^{-1} (respectively 1030 cm^{-1}) over the area of peaks referred to ethylene and methyl groups (reference peaks) and centred at 1460 and 1375 cm^{-1} respectively. The results given in Table 6 of FTIR reveal:

- a gradual increase of carbonyl indices upon ageing. $I_{C=O}$ increases from 2.4% for the fresh bitumen ($B0$) to 6.1% for bitumen recovered from 9-days aged mix $H9$ and to 5.9% for that recovered from 6-days aged warm mix $H6$.
- a gradual increase of sulfoxides $I_{S=O}$ vs. long term ageing time. The $I_{S=O}$ increases from 2.0% for the fresh bitumen ($B0$) to 7.8% for bitumen recovered from 9-days aged mix $H9$ and to 13.3% for that recovered from 6-days aged warm mix $H6$.
- Considering the sum of the two indices as an indicator of ageing ($IC = I_{S=O} + I_{C=O}$), then $IC(B0) = 4.4\%$, $IC(BH9) = 13.9\%$ and $IC(BW6) = 19.2\%$. This means that the bitumen of the warm mix is more oxidized after 6-days ageing than that of the hot mix after 9-days of ageing. As explained before, this is probably due to higher water content (5.5%) used in the foaming process of WMAs.
- a decrease in penetrability, an increase of the softening temperature which are consistent with carbonyl and sulfoxide indices as already observed in the literature [48]
- a gradual increase of the asphaltene content upon ageing duration which is proved to highly influence the stiffness of the bitumen

5 Multiscale modeling

The bituminous mix and bituminous mortar shown in Fig.10 are heterogeneous materials for which we propose to model the linear viscoelastic properties (complex modulus and phase

Bitumen	Pen	T_{RB}	$I_{C=O}(\%)$	$I_{S=O}(\%)$	Asphaltene (%)
B_0	57	49.6	2.4	2.0	13.8
$B(RTFOT163)$	36	55.6	3.3	2.5	15.9
$B(RTFOT163 + PAV)$	21	65.2	6.3	5.4	19.4
$B(H_0)$	37	55.6	4.5	4.2	15.1
$B(H_3)$	30	57.8	5.0	6.2	14.3
$B(H_9)$	26	61.4	6.1	7.8	15.6
$B(RTFOT140)$	45	52.4	2.4	2.7	12.1
$B(RTFOT140 + PAV)$	26	62.4	4.9	6.2	17.0
$B(W_0)$	26	57.0	0.3	11.2	18.7
$B(W_3)$	19	66.2	4.2	12.0	22.4
$B(W_6)$	15	71.8	5.9	13.3	26.7

Table 6: Physico-chemical properties of aged bitumens

angle) using the ECHOES (Extended Calculator of HOmogEnization Schemes) library develop by J-F. Barthélémy and used in previous works [49, 50]. This article is not intended here to present the details of the modeling implemented in ECHOES library, its objective is to use this library to model the properties of asphalt mixes without going into the details of the software.

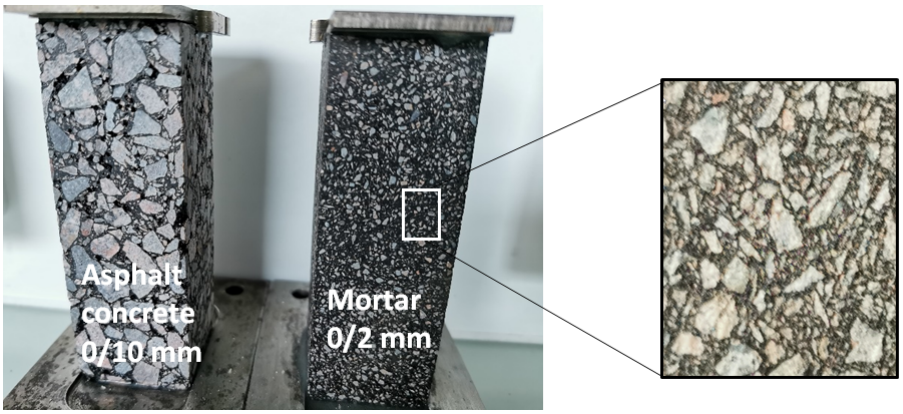

Figure 10: Overview of mortar and bituminous mix specimens

5.1 Input data of the model

Table 5 gives the necessary data concerning the linear viscoelastic properties of the bitumen and the mixes. In addition to these data, the volume fraction f of each constituents relative to the mixture total volume are given in the Table 7. The elastic modulus of aggregates, sands and fines is respectively $E_{ag} = E_{sand} = E_{fines} = 95$ GPa with a Poisson's ratio $\nu_{ag}=\nu_{fines}=\nu_{sand}=0.17$ and a density of $\rho_{ag}=2700\ kg.m^{-3}$. The bitumen bulk modulus $k^{bit}=2500$ MPa and its density is $\rho_{bit}=1040\ kg.m^{-3}$. The voids densty is assumed to be $\rho_{voids}=0\ kg.m^{-3}$. For the warm mixes, the effect of the additive is neglected due to its very low quantity. The aggregates are coated with bituminous mastic film. The nominal mastic film thickness is given by Eq.2.

Mixes	bitumen	fines	sand	2/4	4/6.3	6.3/10	voids
f	12.1%	7.2%	26.6 %	12.1	13.3%	22.7%	6%
Mortar	bitumen	fines	63 μ m/0.5 mm	0.5 mm /1 mm	1 mm / 2 mm		voids
f	22.7%	10.8 %	10.8 %	20.0%	35.5%		0.1%

Table 7: Volume fraction f of the bituminous mixture and mortar constituents

5.2 Representation of the bituminous mix AC 0/10 for the micromechanical purpose

5.2.1 Model description

For the bituminous mixes, the following representative elementary volume ($r.e.v$) is considered and a simplified description of the microstructure is proposed in Fig. 11. All the fractions evoked in this section must be understood as volume fractions.

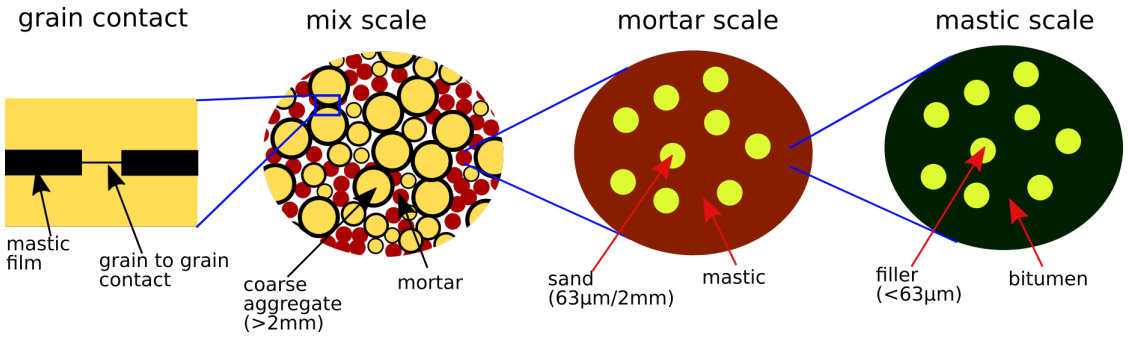

Figure 11: Overview of mortar and bituminous mix specimens

We decompose the bituminous mix into three scales (see Fig.10):

- at the microscale ($0\mu m - 63\mu m$), the mastic is composed of a bitumen matrix embedding fillers. The volume fractions of the bitumen and the fillers are respectively $f_{bit} = 63\%$ and $f_{fines}= 37\%$, whatever the mix formula (HMA, WMA). At the this mastic scale, the Mori-Tanaka (matrix / inclusions) scheme [51] is used because, on the one hand, $f_{bit} \succ f_{fines}$ and of the other hand, the fines are assumed to be surrounded by a connex bituminous phase.

  Let's recall that Eq.2 in section 2.2 assumes that all the bituminous mastic f_{mastic} recovered from experiment is used to coat the aggregates. This is not totally true because only a part of this mastic is used to coat the coarse aggregates and the other part is used to make the bituminous mortar (with the sands) that fills partially the intergranular voids. If one considers that the coarse aggregates are coated by one part α of the bituminous mastic i.e $\alpha \times f_{mastic}$, and the other part of the mastic $(1-\alpha) \times f_{mastic}$ used to make a bituminous mortar, therefore, the thickness of the bituminous mastic film coating the coarse aggregates is no longer governed by the Eq. 2 but rather by the Eq.10.

$$e_{film,mastic}(d_i) = \alpha \times e^{nominal}_{mastic}(d_i) = \alpha \times 61.3 \times (d_i/d_0)^{0.513} \tag{10}$$

  This parameter α brings a correction to the hypothesis behind Eq.2. α is a setting parameter that allows to distribute the bituminous mastic between the mortar and the

mixture. It is evaluated a posteriori.
In Eq.10, d_i represents the mean diameter of the aggregates fraction i (e.g. the aggregates fractions: 2/4, 2/6.3, 6.3/10 in mm ; the mean diameters d_i are respectively 3, 4.15 and 8.15 mm). Thus, the volume fraction of the bituminous mastic used to coat the coarse aggregates at the macroscale $f_{mastic}^{\Gamma_{ag}}$ is determined as follows:

$$f_{mastic}^{\Gamma_{ag}} = \sum_i f_{ag,i} \left(\left(1 + \frac{e_{film,mastic}(d_i)}{d_i/2} \right)^3 - 1 \right) \tag{11}$$

Where $f_{ag,i}$ is the volume fraction of each aggregate fraction.

The volume fraction of the bituminous mastic used to build the mortar at the mesoscale $f_{mastic}^{\subset mortar}$ is then determined as:

$$f_{mastic}^{\subset mortar} = f_{mastic} - f_{mastic}^{\Gamma_{ag}} \tag{12}$$

At the mastic scale, the volume fractions of the mastic portions $f_{mastic}^{\subset mortar}$ used to build respectively the mortar and to coat the coarse aggregates $f_{mastic}^{\Gamma_{ag}}$ are calculated after the optimization process presented in the flowchart see Fig. 12. This leads to respectively: $f_{mastic}^{\Gamma_{ag}}$=1.2% and $f_{mastic}^{\subset mortar}$=98.8% for warm mixes (respectively $f_{mastic}^{\Gamma_{ag}}$=0.2% and $f_{mastic}^{\subset mortar}$=99.8% for hot mixes). These data are independent of the ageing state of the mixes.

- at the mesoscale ($63\mu m - 2mm$), the mortar is composed of a mastic matrix embedding sand grains. This mortar is made with a part of the previous bituminous mastic $f_{mastic}^{\subset mortar}$. In the warm mixes, the volume fractions of the mastic $f_{mastic}^{\subset mortar}$ and sand f_{sand} portions relative to the mortar volume that arise from the flowchart are: $f_{mastic}^{\subset mortar}$= 41.71% and sand f_{sand}=58.29%. For the hot mixes these fractions are respectively $f_{mastic}^{\subset mortar}$=41.92% and sand f_{sand}=58.08%. At the mesoscale, the Mori-Tanaka scheme [51] is used to homogenize the mortar properties since the sand are assumed to be surrounded by the connex bituminous mastic phase.

- at the macroscale ($2mm - 10mm$), the bituminous mix is made of three phases: the coarse aggregates coated with thin bituminous mastic, the mortar phase which partially fills the intergranular and the air voids. The aggregates are represented as spheres coated with bituminous mastic layer whose thickness is given by Eq.10.

  The volume fractions of the warm mixes (WMA) constituents (mortar, pores and coated aggregates) are respectively mortar $f_{mortar}^{\subset mix}$= 45.6%, pores $f_{voids}^{\subset mix}$= 6.0% and coated aggregates $f_{ag}^{\subset mix}$= 48.4% while those of hot mixes are: for the mortar $f_{mortar}^{\subset mix}$= 45.86%, for the pores $f_{voids}^{\subset mix}$= 6.0% and for the coated aggregates $f_{ag}^{\subset mix}$= 48.14%.

  In addition, the bituminous mixture compaction causes contact between the aggregates, which helps to stiffen the granular skeleton of the bituminous mix. This grain-grain contact must be taken into account in the model especially at high temperature or low frequency where the bituminous phase becomes too compliant. Indeed, if the latter is perfectly surrounding the grains (no intergranular contacts), this would entail a large decrease of the overall stiffness in contradiction with experimental measurements. According to an idea proposed in [52], the contact is modeled by a juxtaposition of bitumen

thin layer (of surface fraction χ) and actual grain contacts (of surface fraction $(1-\chi)$). The grain contact does not allow interpenetration of grains but only relative sliding so that it is characterized by a linear spring model relating the local shear stress to the tangential displacement jumps thanks to a shear stiffness k_t. For $\chi = 1$, the grains are entirely surrounded by a thin layer of bitumen, which implies a total loss of stiffness at high temperature or low frequency. On the contrary if $\chi < 1$ such a model is consistent with the idea of connexity of the granular skeleton even at high temperature or low frequency. Finally this model of juxtaposition of bitumen thin layer and grain contacts (see Fig. 11) can be viewed as a composite interphase of thin thickness surrounding the aggregate. It follows from the small thickness that only the out-of-plane components of stress and strain play a mechanical role in this problem so that it is proposed to model the interphase stiffness by the Voigt bound of the two constituents (acting as parallel springs as regards the relevant components of the stiffness tensor). In the frequency domain, i.e. the complex stiffness tensor of the interphase is then written under the form

$$\mathbb{C}^{int} = \chi\,\mathbb{C}^{mastic} + (1-\chi)\,\mathbb{C}^{contact} \text{ with } \mathbb{C}^{contact} = 3\,k^{ag}\,\mathbb{J} + 2\,\alpha\,e_{mastic}\,k_t\,\mathbb{J} \tag{13}$$

where k^{ag} is the bulk modulus of the grain and $\mathbb{J}$ and $\mathbb{K}$ are respectively the spherical and deviatoric fourth-order projectors.

At this macroscale, the generalized self-consistent scheme is used.

5.2.2 Identification of unknown contact and coating parameters

In order to identify the parameters α, χ and k_t that can not be measured by experiment, we minimize the difference between the complex moduli measured E_{2S2P1D} and modeled E^{mod}. We assume that these parameters are not influenced by the ageing. In other words, these parameters are constant for the hot mixes (respectively warm mixes) regardless of the ageing duration (0 to 9 days). These parameters are assumed to depend on the mixing and compaction process. They are determined using the minimization algorithm with inequality constraint COBYLA (Constrained Optimization BY Linear Approximations) [53] (defined as NLOPT.LN_COBYLA in python). This latter allows to find α, k_t, χ shuch that:

$$\sum_{\omega} \left| 1 - \frac{E_{mod}}{E_{2S2P1D}} \right|^2 \leq \varepsilon \text{ with } \varepsilon = 10^{-9} \tag{14}$$

Where ω is the angular frequency in $rad.s^{-1}$
The values of k_t, χ and α that minimize the difference between the multiscale model E_{mod} and the experimental data fitted with 2S2P1D model E_{2S2P1D} are follows:

- for hot mixes (HMA): $\alpha = 5.82 \times 10^{-3}$, $\chi \approx 0.98$ and $k_t \approx 6.1 \times 10^3$;
- for warm mixes (WMA): $\alpha = 4.16 \times 10^{-3}$, $\chi \approx 0.98$ and $k_t \approx 3.7 \times 10^3$

5.2.3 Implementation flowchart

The flowchart Fig. 12 shows the different steps of multiscale modeling described in the previous sections 5.1, 5.2.1 and 5.2.2.

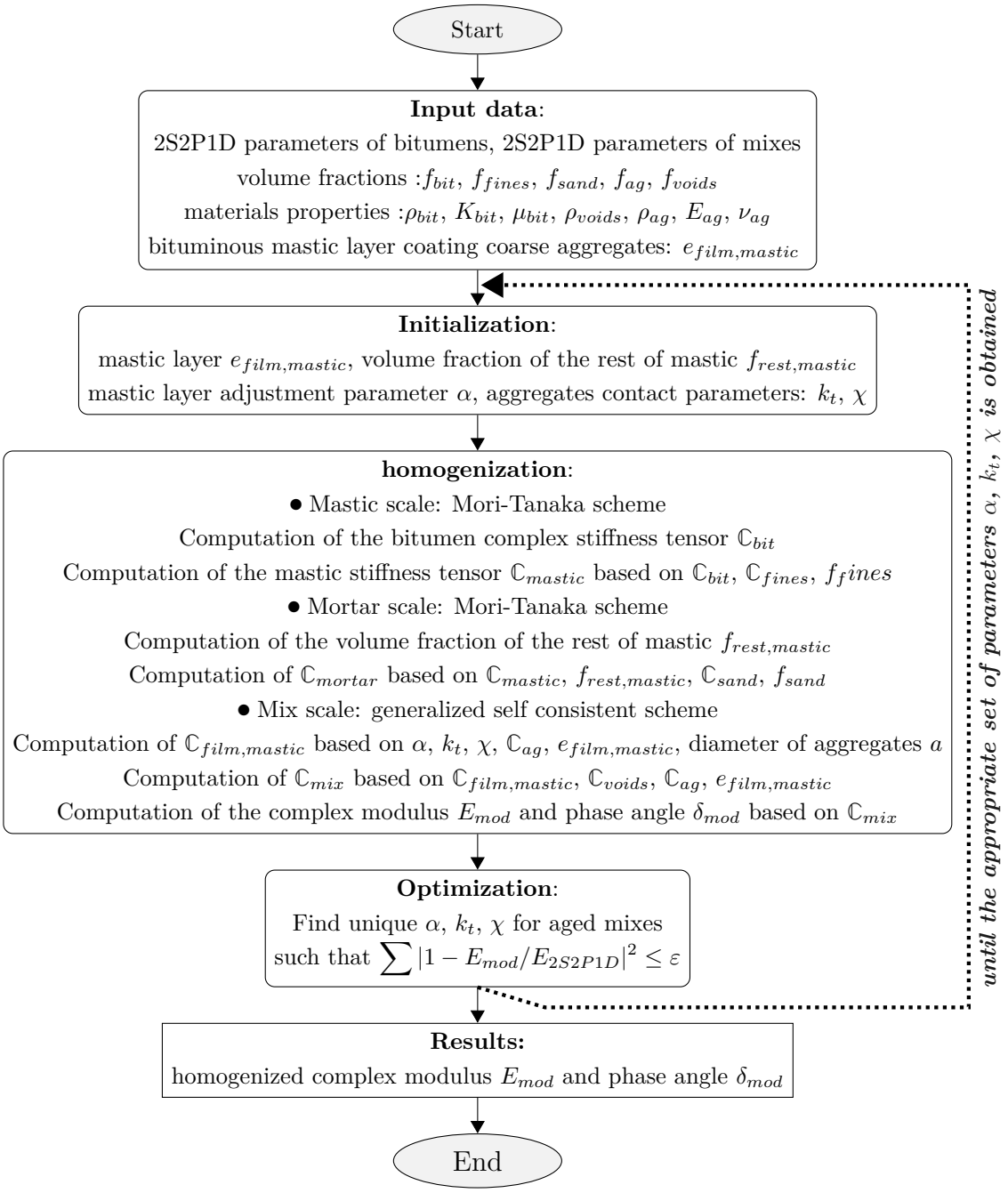

Figure 12: Flowchart of the program implemented

5.2.4 Comparison between the multi-scale model and mixes data

The Figs.13 and 14 show a comparison between the multiscale model and the experimental data curve-fitted with the 2S2P1D model for hot and warm mixes. The Figs.13(a) and Figs.14(a) shows the evolution of the complex modulus according to the frequency of the bitumens and the mixes. The experimental complex modulus of mixes (H0(exp) to H9(exp) for HMA and W0(exp) to W6(exp) for WMA) are compared with the results of the multiscale model that takes into account the grain-grain contact (α, χ and k_t). They are labeled H0(mod) to H9(mod) for HMA and W0(mod) to W6(mod) for WMA. For the value of α, χ and k_t given in section

5.2.2, the model results are in the general trend in good agreement with the experimental results. The same figures Figs.13(a) and Figs.14(a) also show the results of the model with no contact parameters (χ and k_t). It can be seen that at low frequencies the model predicts a significant decrease in the stiffness moduli of some of the mixes. The absence of contact parameters is more visible on the representations of the phase angle δ as a function of the angular frequency ω (Figs.13(b) and 14(b)). It can be observed that, at low frequencies and in the absence of grain-grain contact, the phase angle of the mixture tends asymptotically towards that of the bitumen. This is logical because if the aggregates are perfectly coated with bituminous mastic and if there is no contact between the aggregates, therefore, at low frequencies and high temperatures the properties of the mix, particularly their phase angles tend towards that of the mastic that coat the aggregates. Thus, taking into account the contact parameters makes it possible to take into account the low stiffness of asphalt mixes at high and low temperatures.

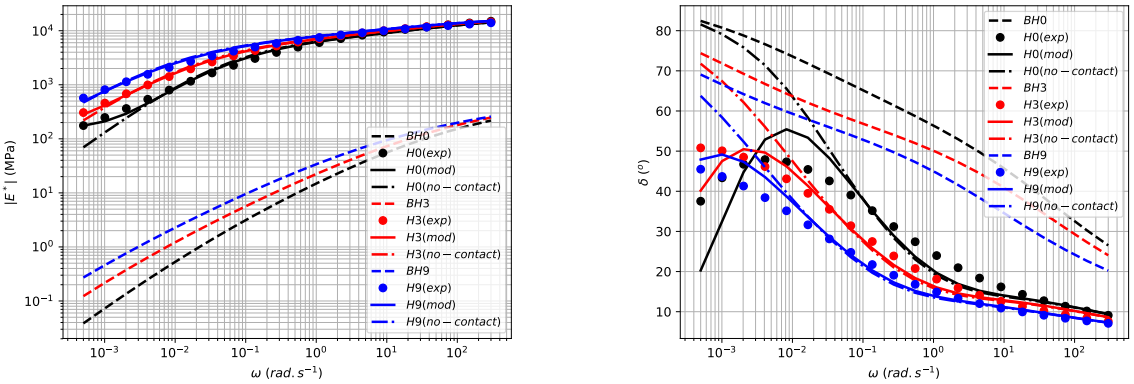

(a) (b)

Figure 13: Comparison between multi-scale model (*mod*) with grain-grain contact and the experiments modeled with 2S2P1D model for HMA

5.3 Case of the bituminous mortar AC 0/2

In this paragraph, we reproduce the previous approach presented in sections 5.2.1 to 5.2.4 to bituminous mortar 0/2 shown on the right side in Fig.10. For this, we decompose the mortar 0/2 into three scales:

For the bituminous mortar, the following representative elementary volume ($r.e.v$) is considered and a simplified description of the microstructure is proposed in Fig.15.

- the microscale ($0\mu m - 63\mu m$), which consists of mastic bituminous made with bitumen matrix and fillers. This bituminous mastic consists of (67.8%) of bitumen and (32.2%) of fines aggregates. Therefore, the Mori-Tanaka (matrix / inclusions) scheme is used at this scale. At the mastic scale the volume fractions of the mastic portions $f_{mastic}^{\subset mortar}$ used to build respectively the mortar and to coat the coarse aggregates $f_{mastic}^{\Gamma_{ag}}$ are calculated after the optimization process presented in the flowchart leads to respectively: $f_{mastic}^{\Gamma_{ag}}$= 2.05% and $f_{mastic}^{\subset mortar}$=97.95%;

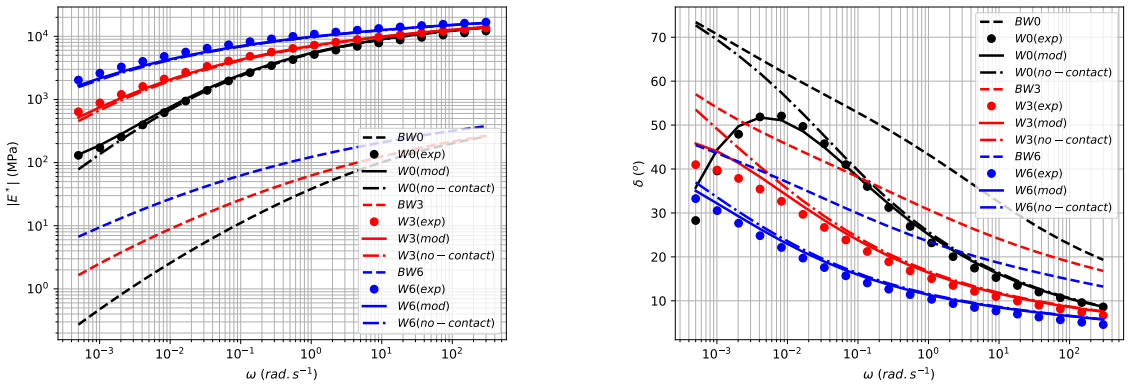

(a) (b)

Figure 14: Comparison between multi-scale model (*mod*) without grain-grain contact and the experiments modeled with 2S2P1D model for WMA

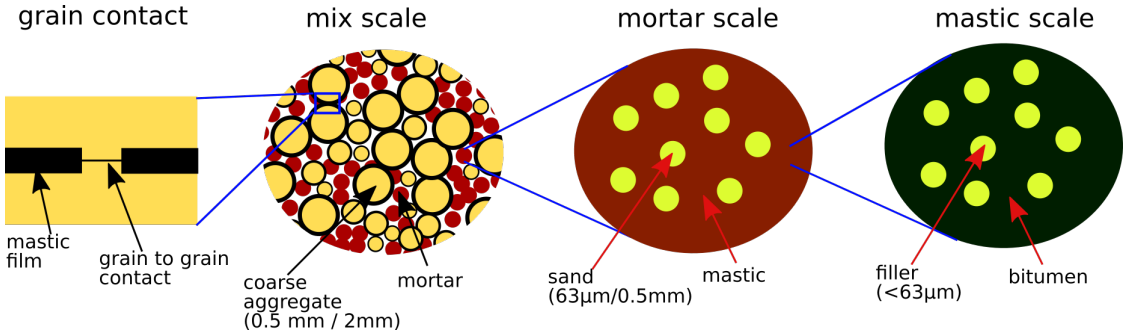

Figure 15: Overview of bituminous mortar specimen

- the mesoscale ($63\mu m - 500\mu m$) where the Mori-Tanaka scheme is used. In the case of AC 0/2, the volume fractions of the mastic $f_{mastic}^{\subset mortar}$ and sand f_{sand} portions relative to the mortar volume that arise from the flowchart are: $f_{mastic}^{\subset mortar}$= 75.64% and sand f_{sand}=24.36%;

- the macroscale ($500\mu m - 2mm$) where the bituminous mix is made of fines aggregates coated with thin bituminous mastic, the mortar phase (build at the mesoscale) fills the intergranular space. At the this scale the grain contact is also allowed between the fines aggregates. At this macroscale, the generalized self-consistent model is used. The volume fractions of the AC 0/2 mix constituents (mortar, pores and coated aggregates) are respectively mortar $f_{mortar}^{\subset mix}$= 44.34%, pores $f_{voids}^{\subset mix}$= 0.1% and coated aggregates $f_{ag}^{\subset mix}$= 55.56%.

The parameters α, χ and k_t determined using the procedure described in the flowchart gives: $\alpha = 0.05$, $\chi = 0.975$ and $k_t = 3.4\times\ 10^3$.

The comparisons between the multiscale model and the and the experimental data curve-fitted with the modified 2S2P1D model for the AC 0/2 mix are shown in Figs.16(a) and Figs.16(b). For the value of α, χ and k_t given above, the model results are in good agreement with the experimental results. The results also highlight a significant decrease in the

predicted stiffness modulus (increase of the predicted phase angle) at low frequencies when the contact parameters are not taken into account.

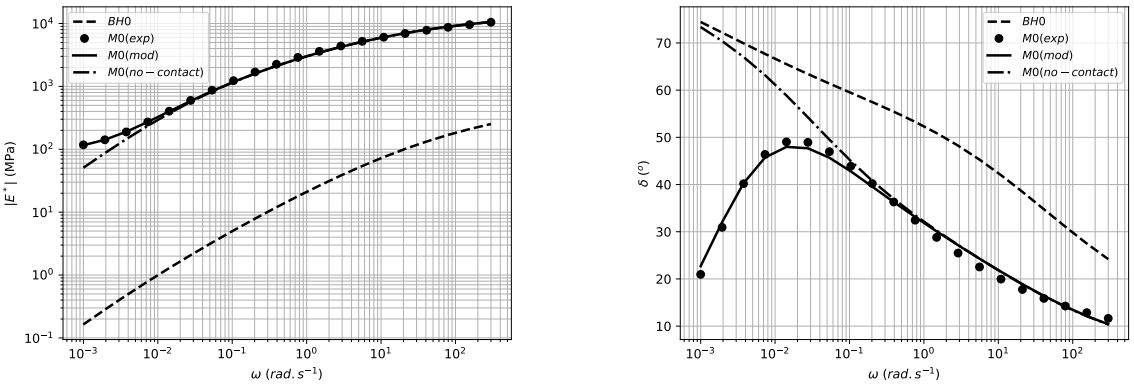

(a) (b)

Figure 16: Comparison between multi-scale model (*mod*) and data for mortar 0/2 mm with and without contact between the aggregates

6 Conclusion

The study presented in this article has two parts: the first part is focused on the impact of long-term ageing kinetics on the linear viscoelastic ($l.v.e.$) properties of bituminous binders and mixes and the second dealt with the multiscale modeling of the properties of these mixes.
In the first part, the effect of long-term kinetic on HMA and WMA is investigated focusing on the evolution of the $l.v.e.$ properties of the binders and the mixes and the chemical assessment of the carbonyl and sulfoxide indexes. The results reveal that:

- the mixes and the binders stiffness moduli increase with the ageing duration. The increase is more pronounced for WMA, probably due to the higher water content used to produce the foam mixture;
- the ageing increases the characteristic time τ of binders and mixes obtained from the modified 2S2P1D models;
- the sulfoxides, carbonyl indices and asphaltene content increase gradually upon ageing ;

In the second part, a multiscale model is implemented to predict the $l.v.e.$ of the mixes based on those of the constituents. It combines a Mori-Tanaka scheme at mastic and mortar scale and generalized self-consistent scheme at the mixture scale with possible grain-grain contact between the aggregates. The reliability of the present multi-scale model is appreciate by comparison with the experimental data. The model predict relatively well the $l.v.e.$ properties of mixes and mortar even at temperatures higher than 30^oC unlike existing, by means of good calibration of the contact parameters k_t, χ and α. These latter can be well calibrated by performing laboratory experiments in a wide range of temperatures.

Declaration of interest statement

This study is not subject to any conflict of interest.

References

[1] Ch. Pichler, R. Lackner, and E. Aigner. Generalized self-consistent scheme for upscaling of viscoelastic properties of highly-filled matrix-inclusion composites - Application in the context of multiscale modeling of bituminous mixtures. Composites: Part B, 43:457–464, 2012.

[2] S.Y. Alam and F. Hammoum. Viscoelastic properties of asphalt concrete using micromechanical self-consistent model. Archives of civil and mechanical engineering, 15:272–285, 2015.

[3] R. Cherif, A. Eddhahak, T. Gabet, F. Hammoum, and J. Nejia. Effect of the processing conditions on the viscoelastic properties of a high-RAP recycled asphalt mixture: micromechanical and experimental approaches. International Journal of Pavement Engineering, 22:708–717, 2021.

[4] B.S. Kambham, V.V. Ram, and S. Raju. Investigation of laboratory and field aging of bituminous concrete with and without anti-aging additives using FESEM and FTIR. Constr. Build. Mat., 222:1193–202, 2019.

[5] CEN EN 12607-1. Bitumen and bituminous binders " Determination of the resistance to hardening under the influence of heat and air " Part 1: RTFOT method. 2014.

[6] CEN EN 14769. Bitumen and bituminous binders " Accelerated long-term ageing conditioning by a Pressure Ageing Vassel (PAV) ". 2013.

[7] F. Xiao, S. N. Amirkhanian, M. Karakouzian, and M. Khalili. Rheology evaluations of WMA binders using ultraviolet and PAV aging procedures. Construction and Building Materials, 79:56–64, 2015.

[8] P. Kandhal and S. Chakraborty. Effect of Asphalt Film Thickness on Short- and Long-Term Aging of Asphalt Paving Mixtures. Transportation research record, 1535:83–90, 1996.

[9] F.C. Martin van de Ven, L.M. Jan Voskuilen, and M.J. Maarten Jacobs. Practical laboratory ageing method dor porous asphalt. 5th Eurasphalt - Eurobitume Congress 13-15th June 2012, 2012.

[10] C. de la Roche, M. Van den bergh, T. Gabet, V. Dubois, J. Grenfell, and L. Porot. Development of a laboratory bituminous mixtures ageing protocol. RILEM Advanced Testing and Characterization of Bituminous Materials, pages 331–345, 2009.

[11] C. Raab, I. Camargo, and M. N. Partl. Ageing and performance of warm mix asphalt pavements. Journal of traffic and transportation engineering, 4(4):388–394, 2017.

[12] G. Van Gooswilligen, F. De Bats, and T. Harrison. Quality of Paving Grade Bitumen - a Practical Approach in Terms of Functional Tests. Proceding 4th Eurobitume Symposium, pages 290–297, 1989.

[13] J. Read and D. Whiteoak. The Shell Bitumen Handbook. 5th London Thomas, page Report, 2003.

[14] Ch. Such, M. Ballié, B. Lombardi, F. Migliori, G. Ramond, J. Samanos, and J.P. Simoncelli. Susceptibilité au vieillissement des bitumes - Expérimentation A08 Groupe national Bitume. Études et recherches des Laboratoires des ponts et chaussées, CR19:163, 1997.

[15] N. Pierard and A. Vanelstrate. Developing a test method for the accelerated ageing of bituminous mixtures in laboratory. RILEM Advanced Testing and Characterization of Bituminous Materials, pages 163–171, 2009.

[16] K. Mollenhauer, V. Mouillet, N. Pierard, M. Tusar, and T. Gabet. Laboratory aging of asphalt mixtures: simulation of reclaimed asphalt and application as test method for durability. 5th Eurasphalt - Eurobitume Congress 13-15th June 2012, 2012.

[17] W. Van den bergh and M.F.C. Van de Ven. The Influence of Ageing on the Fatigue and Healing Properties of Bituminous Mortars. Procedia - Social and Behavioral Sciences, 53:256–265, 2012.

[18] W. Van den bergh and M.F.C. Van de Ven. The Influence of Ageing on the Fatigue and Healing Properties of Bituminous Mortars. Ph.D Thesis, Delft University of Technology, 2011.

[19] CEN TS 12697-52. Bituminous mixtures - Test methods - part 52 : Conditioning to address oxidative ageing. 2017.

[20] C. Nicholls. Analysis of Available Data for Validation of Bitumen Tests. Forum of European National Highway Research Laboratories TRL UK: Report on Phase 1 of the BiTVal Project, page Report, 2006.

[21] C. A. Bell, A.J. Wieder, and M.J. Fellin. Laboratory aging of asphalt-aggregate mixture: field validation. SHRP-A-390, 1994.

[22] A. Collop, Y. Choi, G. Airey, and R. Elliott. Development of a Combined Aging / Moisture Sensitivity Laboratory Test. 3th Eurasphalt - Eurobitume Congress, Vienna, 2004.

[23] Y. Hachiya, K. Nomura, and J. Shen. Accelerated aging tests for asphalt concretes. RILEM Performance Testing and Evaluation of Bituminous Materials, 6th conference, Zurich, 2003.

[24] M. Tia, B.E. Ruth, C.T. Charai, J.M. Shiau, D. Richardson, and J. Williams. Investigation of Original and In-service Asphalt Properties for the Development of Improved Specifications - Final Phase of Testing and Analysis. Final Report, Engineering and Industrial Experiment Station. Gainesville, page Report, 1988.

[25] A. Lachihab. Un modèle numérique pour les composites biphasés matrice - inclusions rigides : Application à la détermination des propriétés élastiques et en fatigue des enrobés bitumineux. PhD, École Nationale des Ponts et Chaussées, 2004.

[26] X-Y. Zhu, Z-X Yang, X-M Guo, and W-Q. Chen. Modulus prediction of asphalt concrete with imperfect bonding between aggregate-asphalt mastic. Composites: Part B, 42:1404–1411, 2011.

[27] X. Shu and B. Huang. Micromechanics-based dynamic modulus prediction of polymeric asphalt concrete mixtures. Composites: Part B, 39:704–713, 2008.

[28] H. Fadil, D. Jelagin, and M. N. Partl. A new viscoelastic micromechanical model for bitumen-filler mastic. Construction and Building Materials, 253:119062, 2020.

[29] L. Eberhardsteiner, J. Fussl, B. Hofko, F. Handle, M. Hospodka, R. Blab, and H. Grothe. Influence of asphaltene content on mechanical bitumen behavior: experimental investigation and micromechanical modeling. Materials and Structures, DOI 10.1617/s11527-014-0383-7, 2014.

[30] J.C. Quezada and C. Chazalon. Complex modulus modeling of asphalt concrete mixes using the Non-Smooth Contact Dynamics method. Computers and Geotechnics, 117:103255, 2020.

[31] H. Feng, M. Pettinari, B. Hofko, and H. Stang. Study of the internal mechanical response of an asphalt mixture by 3-D discrete element modeling. Construction and Building Materials, 77:187–196, 2015.

[32] H. Yu and S. Shen. A micromechanical based three-dimensional DEM approach to characterize the complex modulus of asphalt mixtures. Construction and Building Materials, 38:1089–1096, 2013.

[33] M. Duriez. Traité de matériaux de construction. Dunod, Tome 2, 1950.

[34] E. Hervé and A. Zaoui. N-layered inclusion-based micromechanical modelling. International Journal of Engineering Science, 31:1–10, 1993.

[35] CEN EN 13108-1. Bituminous mixtures. Material specifications. Asphalt Concrete. 2016.

[36] LPC. Extraction des liants d'un enrobé bitumineux pour caractérisation du liant récupéré. Méthode d'essai des LPC, 83.

[37] CEN EN 12697-26. Bituminous mixtures - Test methods - Part 26 : stiffness. 2018.

[38] CEN EN 14770. Bitumen and bituminous binders. Determination of complex shear modulus and phase angle. Dynamic Shear Rheometer (DSR). 2012.

[39] H. C. Booij and G. P. J. M. Thoone. Generalization of Kramers-Kronig transforms and some approximations of relations between viscoelastic quantities. Rheologica Acta, 21 issue 1:15–24, 1982.

[40] E. Chailleux, G. Ramond, C. Such, and C. de La Roche. A mathematical-based master-curve construction method applied to complex modulus of bituminous materials. Road Materials and Pavement Design, 7 sup1:75–92, 2006.

[41] N.W. Tschoegl. The phenomenological theory of linear viscoelastic behaviour. An introduction. Springer-Verlag, New York, pages 143–145, 1989.

[42] C. Huet. Étude par une méthode d'impédance du comportement viscoélastique des matériaux hydrocarbonés. PhD, University Paris 6, 1963.

[43] G. Sayegh. Contribution à l'étude des propriétés viscoélastiques des bitumes purs et des beétons bitumineux. PhD, University Paris 6, 1965.

[44] C. Such. Analyse du comportement visqueux des bitumes. Bulletin de liaison des laboratoires des ponts et chaussées, 127:25–35, 1983.

[45] F. Olard and H. Di Benedetto. General 2S2P1D Model and Relation Between the Linear Viscoelastic Behaviours of Bituminous Binders and Mixes. Road Materials and Pavement Design, 4 Issue 2:185–224, 2003.

[46] A.R. Abbas, M. Nazzal, S. Kaya, S. Akinbowale, B. Subedi, M.S. Arefin, and L.A. Qtaish. Effect of aging on foamed warm mix asphalt produced by water injection. Journal of Materials in civil Engineering, 28:1–11, 2016.

[47] N. Li, W. Tang, X. Yu, H. Zhan, H. Ma, G. Ding, and Y. Zhang. Investigation of moisture dissipation of water-foamed asphalt and its influence on the viscosity. Materials, 13:1–11, 2020.

[48] G. Pipintakos, H.Y.V. Ching, H. Soenen, P. Sjovall, U. Muhlich, S. Van Doorslaer, A. Varveri, W. Van den bergh, and X. Lu. Experimental investigation of the oxidative ageing mechanisms in bitumen. Construction and Building Materials, 260:119702, 2020.

[49] J-F. Barthélémy, A. Giraud, F. Lavergne, and J. Sanahuja. The Eshelby inclusion problem in ageing linear viscoelasticity. International Journal of Solids and Structures, 97-98:530–542, 2016.

[50] J.-F. Barthélémy, A. Giraud, J. Sanahuja, and I. Sevostianov. Effective properties of ageing linear viscoelastic media with spheroidal inhomogeneities. IInternational Journal of Engineering Science, 144:103104, 2019.

[51] L. Dormieux, D. Kondo, and F-J Ulm. Microporomechanics. John Wiley & Sons, 2006.

[52] H. Di Benedetto and F. Olard. Linear viscoelastic behaviour of bituminous materials: From binders to mixes. Road Materials and Pavement Design, 5 Sup 1:163–202, 2004.

[53] M.J.D Powell. Direct search algorithms for optimization calculations. Acta Numerica, 7:287–336, 1998.

Nomenclature

HMA: hot mix asphalt
WMA: warm mix asphalt
ρ: density, $kg.m^{-3}$
d: aggregate diameter, mm
S: specific surface
e: mastic film thickness, μm
f: frequency, Hz
ω: angular frequency, $rad.s^{-1}$
δ: phase angle, ^{o}
G^*: shear modulus, MPa
E^*: stiffness modulus, MPa
E_1,E_2: real, imaginary part of E^*, MPa
G_1,G_2: storage, loss shear modulus, MPa
M_t: Torque moment, N.m
a_T: shift factor
T_{ref}: reference temperature, ^{o}C
T: temperature, ^{o}C
R: radius of specimen in DSR, mm
H: thickness of bitumen specimen, mm
C_1,C_2: coefficients of WLF law
E_0,E_∞: static, glassy modulus, MPa
δ,β,τ: 2S2P1D parameters
η: Newtonian viscosity of the 2S2P1D parameters
IC: ageing indicator
ν: Poisson's ratio
k,h: modified 2S2P1D models parameters
k^{bit},k^{ag}: bulk modulus, MPa
I_{CO},I_{SO}: carbonyl, sulfoxide indexes
ϵ: strain
ϵ: sum of residuals
χ,k_t: grain-grain contact parameter
f: volume fraction %
E_{mod}: homogenized stiffness modulus
z_0: amplitude of displacement in 2P-PR test m
z: displacement in 2P-PR test m
μ: mass factor in 2P-PR test
γ: specimen form factor in 2P-PR test
F: force in 2P-PR test
m: mass of the movable part of 2P-PR device
M: mass of the prismatic specimen in 2P-PR test
b,L,h: prismatic specimen dimension in 2P-PR test
$\mathbb{C}$: stiffness tensor
$\mathbb{J}$, $\mathbb{K}$: spherical and deviatoric fourth-order projectors